Broadband Microwave Photonic Mixer With High Spurs Suppression and Image Rejection

Gai Shen and Yue Zhou

***Abstract*—A microwave photonic mixer for up- and down-conversion based on dual parallel in-phase and quadrature (I/Q) modulators is proposed. Dual parallel I/Q modulators and 90-degree electrical hybrid couplers are used to obtain carrier-suppressed single-sideband modulation of radio frequency (RF), intermediate frequency (IF), and local oscillator (LO) signals. The optical bandpass filter (OBPF) is employed to select the −1st-order or +1st-order sideband of the LO signal to realize up and down conversion. In the experiments, an IF frequency range of 5–17 GHz can be upconverted to an RF frequency range of 15–37 GHz, and an RF frequency range of 8–40 GHz can be downconverted to an IF frequency range of 2–5 GHz. The spurs suppression ratio exceeds 50 dB for up and down conversion. To the best of our knowledge, this is the highest reported spurs suppression in a broadband microwave photonic mixer. Moreover, the OBPF is also utilized to obtain an image rejection ratio (IRR) of 45.91 dB at an IF frequency of 4 GHz. To obtain a lower frequency of IF signal and a higher IRR, a Brillouin-assisted notch filter is applied to attenuate the image signal. In this way, an IRR of more than 60 dB can be obtained at an IF frequency of 2 GHz.**

***Index Terms*—Frequency conversion, image rejection mixer, microwave photonics, stimulated Brillouin scattering (SBS).**

I. Introduction

MICROWAVE photonic mixer is of prime importance in modern microwave and millimeter wave systems. Compared with traditional electrical systems, microwave photonic techniques become increasingly attractive because of their intrinsic metrics of large bandwidth and immunity to electromagnetic interference. Inspired by the above advantages, microwave photonic mixer continues to provide solutions to potential applications in radar, radio over fiber (RoF) systems, and satellite payload [1], [2], [3]. Several microwave photonic-based broadband frequency converters have been proposed and demonstrated in recent years [4], [5]. In previous methods, frequency downconversion based on double-sideband (DSB) modulation can be realized by cascading two Mach-Zehnder modulators (MZM) [6]. However, the downconverted signal has a lot of spurs since the carrier has not been effectively suppressed, which causes limited local oscillator (LO)–radio frequency (RF) isolation. The suppression of useless signals can be achieved with carrier-suppressed double-sideband (CS-DSB) modulation [7], [8]. This solution is only capable of achieving down-conversion and still remaining certain mixing spurs. To further reduce the mixing spurs, carrier-suppressed single-sideband (CS-SSB) modulation has been proposed in [9], [10], [11], [12], [13]. Moreover, up and down conversion can be achieved simultaneously by selecting the +1st or -1st-order sideband of the LO signal. Although CS-SSB modulation of RF signal has been obtained in [13], the frequency conversion is also achieved with CS-DSB frequency doubled LO signal, which leads to a low spurs suppression ratio of 19 dB.

In the down-conversion process, frequencies spaced equally above and below the LO are downconverted to the same intermediate frequency (IF). As a result, the undesired image product interferes with the desired signal, degrading the performance of the mixer [7], [14]. The microwave photonics-based image rejection mixer (IRM) is developed to eliminate the undesired signal from the image, which also exhibits a larger bandwidth when compared to traditional electrical IRM [15]. The method of pre-filtering for image rejection employs electrical bandpass filter (EBPF) to filter out image signal in the electrical domain [16] and optical bandpass filter (OBPF) to select useful RF sideband in the optical domain [17]. However, it is necessary to use the EBPF and OBPF with a broad operating frequency range, wide tunability, and sharp edge roll-off to obtain a higher image rejection ratio (IRR). Although the multiple-stage frequency conversion avoids the use of rare BPF, many electro-optical modulators and erbium-doped fiber amplifiers (EDFAs) are contained in this method, increasing the cost and complexity of the system [18].

An alternative approach for achieving IRM is Hartley architecture, which is implemented by the in-phase enhan-cement of useful signals and the out-of-phase cancelation of undesired image signals [19], [20], [21], [22], [23], [24]. The performance of IRM based on Hartley architecture depends on the accuracy of the phase and amplitude between two quadrature IFs. Path mismatch or environmental variation may lead to reduced accuracy [9]. The latest microwave photonic mixer based on the Hartley architecture has been reported in [20]. Exper-imental results indicate an image frequency rejection of over 60 dB, with an operating frequency ranging from 5 to 20 GHz.

Moreover, the stimulated Brillouin scattering (SBS) effect is introduced into the IRMs [25], [26], [27], [28], [29]. The SBS gain spectrum of the pump light is used to amplify

Manuscript received 30 October 2023; revised 17 December 2023; accepted 23 December 2023. Date of publication 27 December 2023; date of current version 5 January 2024. This work was supported by the National Key Research and Development Program Key Special Project of China under Grant 2021YFF0901700. *(Corresponding author: Yue Zhou.)*

The authors are with the State Key Laboratory of Information Photonics and Optical Communications, School of Electronic Engineering, Beijing University of Posts and Telecommunications, Beijing 100876, China (e-mail: shengai@bupt.edu.cn; yuezhou@bupt.edu.cn).

Digital Object Identifier 10.1109/JPHOT.2023.3347709

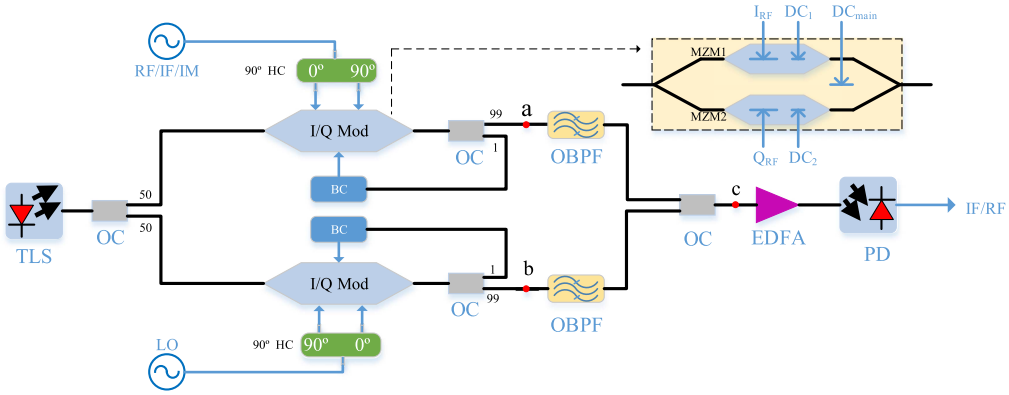

Fig. 1. Schematic diagram of the proposed dual parallel I/Q modulators-based microwave photonic mixer. IM, image; TLS, tunable laser; OC, optical coupler; I/Q Mod, in-phase and quadrature modulator; BC, bias control; HC, hybrid coupler; OBPF, optical bandpass filter; EDFA, erbium-doped fiber amplifier; PD, photodetector; MZM, mach-zehnder modulator.

the +1st-order RF sideband [27] while the loss spectrum is utilized to attenuate the -1st-order RF sideband. As a result, the IF from the undesired image interferes destructively whereas the IF from the desired RF signal is enhanced [28]. Nevertheless, the SBS noise with the same frequency as the RF sideband is induced, and the RF pump signal is still needed for frequency conversion when the image signal is absent. A Brillouin-assisted notch filter-based IRM is presented in [29]. The image signal is attenuated by the loss spectrum of the pump light without affecting the RF sideband. However, the +1st-order image sideband is not completely suppressed, which results in a limited IRR of 32 dB.

In this article, we propose and demonstrate a broadband microwave photonic mixer with a high spurs suppression ratio and IRR, which also does not suffer from the path mismatch problem. Dual parallel in-phase and quadrature (I/Q) modulators and 90-degree electrical hybrid couplers (HCs) are used to obtain CS-SSB modulation signals of RF, LO, and IF. The upper or lower sideband of LO is selected by the tunable OBPF to realize up or down conversion. Image rejection is implemented by the OBPF, too. In the experiments, an IF frequency range (5–17 GHz) can be upconverted to an RF frequency range (15–37 GHz). An RF frequency range (8–40 GHz) can be downconverted to an IF frequency range (2–5 GHz). For both up and down-conversion, the spurs suppression ratio is over 50 dB while the conversion gain is approximately −33 dB. The IRR reaches 45.91 dB at an IF frequency of 4 GHz. To acquire a lower frequency of downconverted signal and a higher IRR, a Brillouin-assisted notch filter is applied to attenuate the image signal. In this case, an IRR of more than 60 dB can be obtained at an IF frequency of 2 GHz. With its high spurs suppression ratio and IRR, the proposed mixer is well-suited for applications in radar receiver, RoF system, electronic warfare, and satellite payload. The integration of the modulators and SBS medium used in this study has already been reported [30]. Therefore, the microwave photonic mixer proposed in this article has the potential for integration in the future.

II. Principle

A. Up- and Down-Converter

The structure of the proposed microwave photonic mixer is shown in Fig. 1. A tunable laser (TLS) is used as the laser source, and the optical carrier is fed into two completely symmetrical branches with an optical coupler (OC). In the upper branch, the bias control module is employed to control the I/Q modulator to achieve CS-SSB modulation of the RF/IF signal. In the lower branch, the CS-SSB signal of LO can be obtained in the same way. Assuming that the extinction ratio of the I/Q modulator is infinite and the insertion loss of devices is ignored, the output optical field of the lower and the upper I/Q modulator can be written as

$$\begin{aligned} E_L(t) &= E_{MZM1} + E_{MZM2}e^{j\varphi_1} \\ &= \frac{\sqrt{2}}{8}E_0 e^{j2\pi f_c t} \\ &\cdot \left\{ \begin{array}{l} [e^{jm_{LO}\cos 2\pi f_{LO}t} + e^{j(-m_{LO}\cos 2\pi f_{LO}t+\varphi_2)}] \\ +[e^{jm_{LO}\sin 2\pi f_{LO}t} + e^{j(-m_{LO}\sin 2\pi f_{LO}t+\varphi_2)}]e^{j\varphi_1} \end{array} \right\} \\ &= \frac{\sqrt{2}}{2}E_0 J_1(m_{LO}) e^{j2\pi(f_c \pm f_{LO})t + j\frac{\pi}{2}}, \varphi_1 = \pm\frac{\pi}{2}\ \varphi_2 = \pi \end{aligned} \tag{1}$$

$$E_U(t) = \frac{\sqrt{2}}{2}E_0 J_1(m_{Sig}) e^{j2\pi(f_c + f_{Sig})t + j\frac{\pi}{2}}, \varphi_1 = +\frac{\pi}{2}\ \varphi_2 = \pi \tag{2}$$

where E_0 and f_c are the amplitude and frequency of the optical carrier. φ_1 is the phase difference between two sub MZMs, φ_2 is the phase difference between two arms of a single MZM. Different sidebands can be obtained by changing the polarity of φ_1 through the alteration of the voltage polarity output from the bias control module. f_{Sig} and f_{LO} are the frequency of the RF/IF signal and LO signal respectively, m_{Sig} and m_{LO} are the modulation indices, and $J_1(m_{Sig})$ is the first-order Bessel

function of the first kind. The sidebands with the order higher than 2nd are neglected under small signal modulation.

Tunable OBPF is utilized to select the upper or lower sideband of LO to achieve down- or up-conversion as shown in Fig. 2. The upconverted and downconverted signals can be expressed as

$$i_U \propto \frac{1}{4} G_0 \Re J_1(m_{IF}) J_1(m_{LO}) \cos 2\pi (f_{IF} + f_{LO}) t \quad (3)$$

$$i_D \propto \frac{1}{4} G_0 \Re J_1(m_{RF}) J_1(m_{LO}) \cos 2\pi (f_{RF} - f_{LO}) t \quad (4)$$

where G_0 denotes the optical gain introduced by EDFA, $\Re$ denotes the responsivity of the photodetector (PD), m_{RF} and m_{IF} are the modulation indices, and f_{RF} and f_{IF} are the fre-quencies of RF signal and IF signal, respectively.

B. Pre-Filtering Based Image Rejection Mixer

When the image signal is applied to the upper I/Q modulator and under the assumption that the frequency of the downconverted IF signal exceeds the bandwidth of the OBPF, the image signal can experience maximum out-of-band suppression. In the upper branch, the output optical field of the OBPF can be expressed as

$$E_{OBPF}(t) = \frac{\sqrt{2}}{2} E_0 e^{j\frac{\pi}{2}} \times \begin{bmatrix} J_1(m_{RF}) e^{j2\pi(f_c + f_{RF})t} \\ + \sqrt{L_F(f_c + f_{IM})} J_1(m_{IM}) e^{j2\pi(f_c + f_{IM})t} \end{bmatrix} \quad (5)$$

where f_{IM} denotes the frequency of the image signal, and $L_F(f_c + f_{IM})$ denotes the out-of-band suppression at a frequency of $f_c + f_{IM}$ introduced by OBPF. The signal before PD can be expressed as

$$E_{PD}(t) = \frac{\sqrt{2}}{2} E_0 \sqrt{G_0} \times \begin{bmatrix} J_1(m_{RF}) e^{j2\pi(f_c + f_{RF})t} \\ + J_1(m_{LO}) e^{j2\pi(f_c + f_{LO})t + j\frac{\pi}{2}} \\ + J_1(m_{IM}) \sqrt{L_F(f_c + f_{IM})} e^{j2\pi(f_c + f_{IM})t} \end{bmatrix} \quad (6)$$

After detection in PD, the photocurrent of the IF signal from the desired RF signal and undesired image signal can be expressed as:

$$i_{RF} \propto E_0^2 G_0 J_1(m_{RF}) J_1(m_{LO}) \cos 2\pi f_{IF} t \quad (7)$$

$$i_{IM} \propto E_0^2 G_0 \sqrt{L_F(f_c + f_{IM})} J_1(m_{IM}) J_1(m_{LO}) \cos 2\pi f_{IF} t \quad (8)$$

The IRR can be written as

$$IRR \propto \frac{J_1(m_{RF})^2}{J_1(m_{IM})^2 L_F(f_c + f_{IM})} \quad (9)$$

From (9), the IRR is entirely dependent on the out-of-band suppression of the image signal when the RF signal and the image signal have the same power. Nevertheless, the image signal cannot be completely suppressed when the frequency of the IF signal approaches the bandwidth of the OBPF, which causes a reduction in IRR. To improve the mixing performance of the proposed scheme, another IRM based on SBS is proposed.

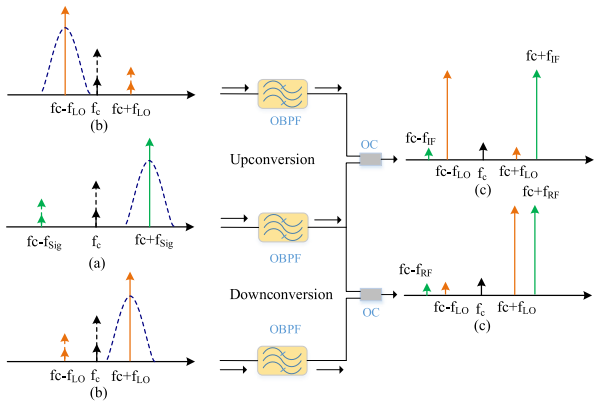

Fig. 2. Simplified optical spectra at different points in Fig. 1 under different conversion modes. (a) Optical spectra of the RF/IF signal. (b) Optical spectra of the LO signal. (c) Optical spectra after the optical coupler. f_{RF} is the frequency of the RF signal, f_c is the frequency of the optical carrier, f_{LO} is the frequency of the LO signal, f_{Sig} is the frequency of the RF/IF signal.

C. Stimulated Brillouin Scattering-Based Image Rejection Mixer

The structure of the proposed SBS-based IRM is shown in Fig. 3. Another OC is inserted after TLS to divide part of the optical power to generate pump light. In the upper branch, a bias control module is employed to control the intensity modulator to implement CS-DSB modulation, and the resulting pump light is amplified by the EDFA. In the middle branch, the forward-transmitted optical signal interacts with the counter-propagating amplified pump light in the single-mode fiber (SMF) as shown in Fig. 4. The RF pump frequency is set to f_p, and the optical carrier frequency is f_c, as a result, the pump has two sidebands which have the frequency of $f_c + f_p$ and $f_c - f_p$, respectively. Each sideband of the pump introduces both the SBS gain and loss spectrum. Only the loss spectrum introduced by the +1st-order pump sideband is used in this experiment. To attenuate the +1st-order sideband of the image, the image sideband should be located at the center of the loss spectrum introduced by the +1st-order sideband of the pump signal as shown in Fig. 4. Therefore, the frequency of the image signal should be equal to $f_p + f_B$, where f_B is the Brillouin frequency shift. To better understand the principle of the proposed SBS-based IRM, a theoretical analysis is carried out. Assuming that the extinction ratio of the I/Q modulator is infinite and the insertion loss of devices is ignored, in order to attenuate the +1st-order sideband of the image signal, fp is set to

$$f_p = f_{IM} - f_B \quad (10)$$

In the middle branch, the +1st-order sidebands of RF and image can be acquired by the previous method. After the SBS process, the +1st-order sideband of RF remains unchanged

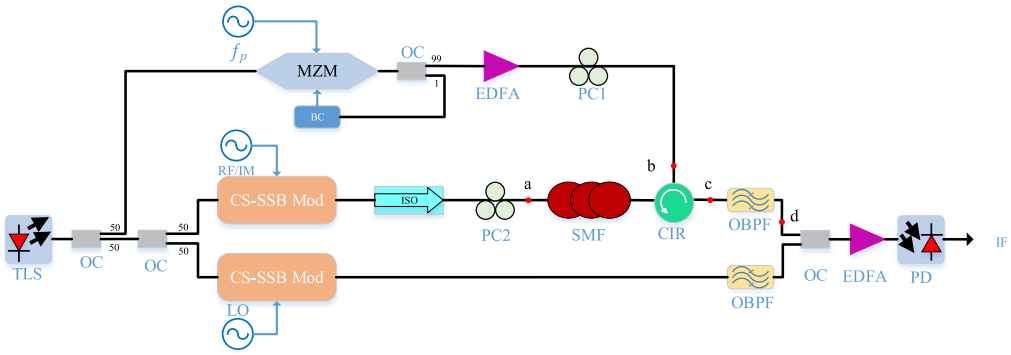

Fig. 3. Schematic diagram of the proposed SBS-based image rejection mixer. IM, image; TLS, tunable laser; OC, optical coupler; CS-SSB Mod, carrier-suppressed single-sideband modulator; BC, bias control; OBPF, optical bandpass filter; EDFA, erbium-doped fiber amplifier; PD, photodetector; MZM, mach-zehnder modulator, intensity modulator is used here; SMF, single-mode fiber; PC, polarization controller; CIR, circulator; ISO, isolator.

while the +1st-order sideband of the image is attenuated. The OBPF is employed to filter out the remaining +1st-order image sideband and select the desired +1st-order RF sideband. The signal after OBPF can be expressed as

$$E_M(t) = \frac{1}{2}E_0 e^{j\frac{\pi}{2}}\sqrt{L_S} \times \begin{bmatrix} J_1(m_{RF})e^{j2\pi(f_c+f_{RF})t} \\ +J_1(m_{IM})\sqrt{L_F(f_c+f_{IM})} \\ \cdot A(f_c+f_{IM})e^{j[2\pi(f_c+f_{IM})t+\Phi(f_c+f_{IM})]} \end{bmatrix} \quad (11)$$

where L_S is the optical loss introduced by SMF, $A(f_c + f_{IM})$ and $\Phi(f_c + f_{IM})$ are the SBS amplitude loss and the SBS induced phase shift at $f_c + f_{IM}$, and $\Phi(f_c + f_{IM}) = 0$ when (10) is satisfied. The signal before PD can be expressed as

$$E'_{PD}(t) = \frac{1}{2}E_0\sqrt{G_0}\sqrt{L_S}e^{j\frac{\pi}{2}} \times \begin{bmatrix} J_1(m_{RF})e^{j2\pi(f_c+f_{RF})t} \\ +J_1(m_{LO})e^{j2\pi(f_c+f_{LO})t+j\frac{\pi}{2}} \\ +J_1(m_{IM})\sqrt{L_F(f_c+f_{IM})} \\ \cdot A(f_c+f_{IM})e^{j2\pi(f_c+f_{IM})t+j\Phi(f_c+f_{IM})} \end{bmatrix} \quad (12)$$

After detection in PD, the photocurrent of the IF signal from the desired RF signal and undesired image signal can be expressed as

$$i'_{RF} \propto E_0^2 L_S G_0 J_1(m_{RF}) J_1(m_{LO}) \cos 2\pi f_{IF} t \quad (13)$$

$$i'_{IM} \propto E_0^2 L_S G_0 \sqrt{L_F(f_c+f_{IM})} A(f_c+f_{IM}) \cdot J_1(m_{IM}) J_1(m_{LO}) \cos 2\pi f_{IF} t \quad (14)$$

IRR can be written as

$$IRR' \propto \frac{J_1(m_{RF})^2}{L_F(f_c+f_{IM})A(f_c+f_{IM})^2 J_1(m_{IM})^2} \quad (15)$$

From (15), the IRR of the proposed improved scheme is contingent not only on the notch depth of the loss spectrum but also on the suppression of the image introduced by OBPF. Additionally, due to the use of the CS-DSB pump, the -1st-order sideband of the pump is utilized to attenuate the image signal instead of the +1st-order sideband when the frequency of the RF signal is less than the Brillouin frequency shift. As a result, an additional loss spectrum introduced by the +1st-order pump sideband will appear at a frequency higher than the attenuated image signal. This additional loss spectrum may attenuate the useful RF sideband. Therefore, the operating frequency of the proposed SBS-based IRM is restricted above the Brillouin frequency shift [29].

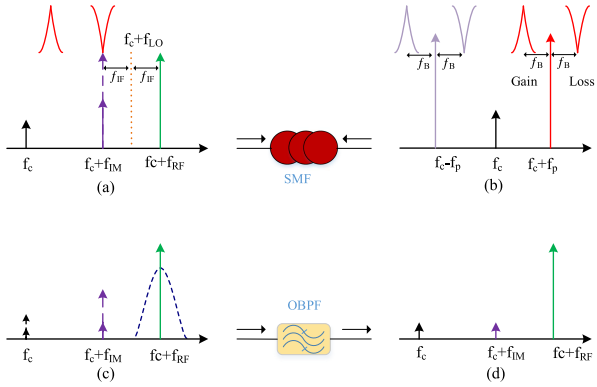

Fig. 4. Simplified optical spectra at different points in Fig. 3. (a) Optical spectra before the single-mode fiber. (b) Optical spectra of the pump light. (c) Optical spectra after the SBS process. (d) Optical spectra after the OBPF, whose frequency response was marked as blue dashed line in (c). f_B is the brillouin frequency shift, f_{RF} is the frequency of the RF signal, f_c is the frequency of the optical carrier, f_p is the frequency of the pump signal, f_{IM} is the frequency of the image signal, f_{LO} is the frequency of the LO signal, f_{IF} is the frequency of the IF signal.

III. Experiment and Result

Experiments based on the setup shown in Fig. 1 are carried out to verify the proposed scheme. A polarization-maintaining continuous wave light with 25 kHz linewidth and 16 dBm optical power from a TLS (CoBrite CBDX2) was split into two paths via a 50:50 OC. In the upper branch, the optical carrier was launched into an I/Q modulator (EOspace IQ-0DVS). The RF/IF signal was generated by the microwave source (Agilent E8257D). Upon passing through the 90-degree electrical HC (GT CT-CP), the electrical signal was split into two quadrature signals, which were connected to the I_{RF} and Q_{RF} ports of the I/Q modulator. Additionally, 1% optical power was provided as optical feedback

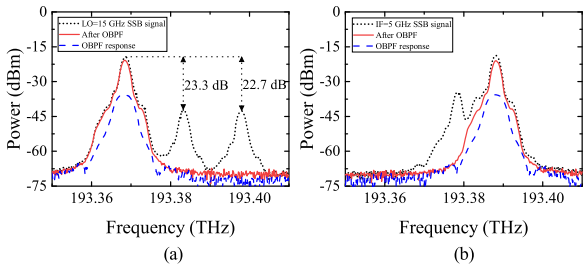

Fig. 5. Measured optical spectra in the (a) lower and (b) upper branch in upconversion before OBPF (black dotted line) and after OBPF (red solid line). Response of OBPF (blue dashed line).

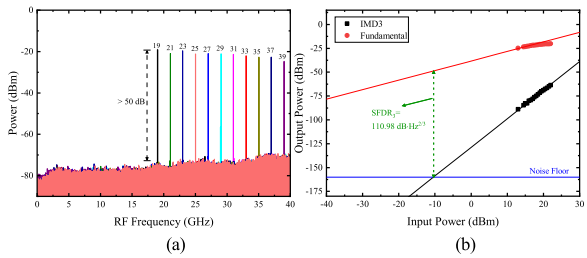

Fig. 6. Measured (a) electrical spectra of the upconverted signals when the IF frequency was fixed at 9 GHz and the LO frequency varied from 10 to 30 GHz and (b) spurious-free dynamic range for upconversion.

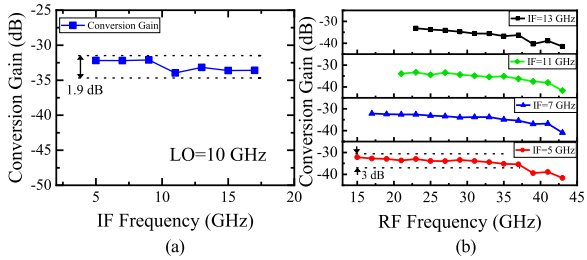

Fig. 7. Measured (a) conversion gain versus IF frequency when LO frequency was fixed at 10 GHz and (b) conversion gain versus RF frequency for different IF frequencies in upconversion.

to the bias control module (Plug-Tech MBC-IQ) via a 1:99 OC. The bias control module was employed to control the sub-MZM1, sub-MZM2, and main-MZM of the I/Q modulator to work at minimum transmission point (MITP), MITP, and quadrature transmission point (QTP) respectively to achieve CS-SSB modulation. 99% of the optical power was injected into a tunable OBPF (TeraXion TFN) with an out-of-band suppression of over 25 dB and a bandwidth of 4 GHz. The tunable OBPF was utilized to select the desired signal and suppress the image and other harmonic spurs. In the lower branch, the CS-SSB signal of LO can be acquired in the same way. The optical signals from both branches were combined via an OC and injected into an EDFA (Amonics AEDFA) with 30 dB optical gain. The amplified signal was detected by a PD (u2t GT-XPDV2120R). Furthermore, up and down frequency conversion can be realized by altering the voltage polarity applied to the main MZM of the lower I/Q modulator.

A. *Up-Converter*

To realize frequency upconversion, the -1st-order sideband of LO and the +1st-order sideband of IF should be obtained in the lower and upper branches. To obtain the -1st-order sideband of LO, the voltage polarity applied to the main MZM of the lower I/Q modulator was altered through the bias control module, while the +1st-order sideband of IF was acquired without changing the voltage polarity in the upper I/Q modulator. In order to showcase the performance of CS-SSB modulation, the frequency of the optical carrier was set to 193.38 THz (1550.27 nm) with an optical power of 16 dBm. The IF frequency was set to 5 GHz with a power of 13 dBm. The frequency and power of the LO signal were 15 GHz and 17 dBm, respectively. The optical spectra of the lower branch and the upper branch were shown in Fig. 5(a) and (b) respectively. As can be seen, a sideband suppression ratio of 22.7 dB and a carrier suppression ratio of 23.3 dB can be obtained. In addition, the +1st-order sideband of IF and the -1st-order sideband of LO were selected by the tunable OBPF, whose frequency response was marked as blue dotted line in Fig. 5(a) and (b). Meanwhile, the optical carrier and other unwanted sidebands were suppressed under the noise floor.

The electrical spectra of the upconverted RF signal were measured when the IF frequency was fixed at 9 GHz and the LO frequency varied from 10 to 30 GHz. As can be seen from Fig. 6(a), the mixing spurs were completely suppressed under the noise floor within a frequency span of 40 GHz, the corresponding spurs suppression ratio exceeding 50 dB. It is worth noting that the signal power decreased at an RF frequency of 39 GHz since the responsivity of the PD was reduced when a high-frequency signal (∼38 GHz) was applied. The spurious-free dynamic range (SFDR) for upconversion was measured by introducing two-tone IF signals at 10 GHz and 10.1 GHz, and the LO frequency was set to 8 GHz. As can be seen in Fig. 6(b), a noise floor at -160 dBm/Hz was assumed, and the SFDR was about 110.98 dBc·Hz$^{2/3}$.

Fig. 7(a) shows the conversion gain versus IF frequency when the LO frequency was fixed at 10 GHz and the IF frequency was adjusted from 5 to 17 GHz. As can be seen, the conversion gain remained near -33 dB with a fluctuation of 1.9 dB. Furthermore, the conversion gain as a function of upconverted RF frequency for different IF frequencies was measured in Fig. 7(b). As can be seen, a frequency range (5–17 GHz) of IF can be upconverted to a frequency range (15–37 GHz) of RF when the fluctuation of conversion gain was 3 dB. Nevertheless, the conversion gain decreased when the RF frequency was higher than 39 GHz, which was attributed to the reduced responsivity of PD.

B. *Down-Converter*

To achieve frequency downconversion, the +1st-order sidebands of RF and LO should be acquired in the upper and lower branches, respectively. The frequency (193.38 THz) and power (16 dBm) of the optical carrier were consistent with the upconversion mode. In order to showcase the performance of CS-SSB modulation, the RF frequency was set to 23 GHz with a power of 13 dBm, and the frequency and power of the LO signal

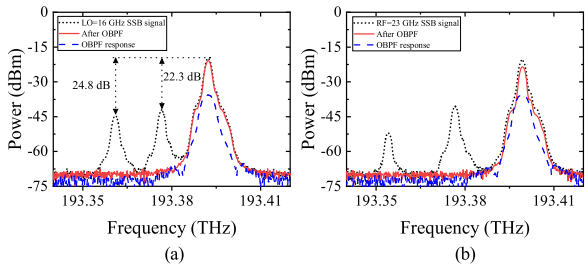

Fig. 8. Measured optical spectra in the (a) lower and (b) upper branch in downconversion before OBPF (black dotted line) and after OBPF (red solid line). Response of OBPF (blue dashed line).

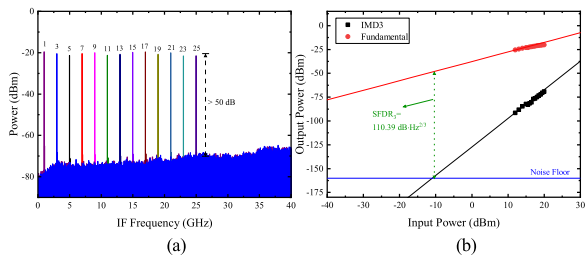

Fig. 9. Measured (a) electrical spectra of the downconverted signals when the LO frequency was fixed at 15 GHz and the RF frequency varied from 16 to 40 GHz and (b) spurious-free dynamic range for downconversion.

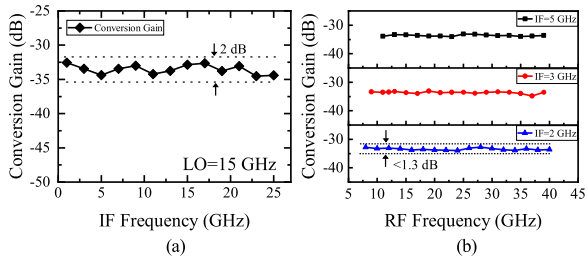

Fig. 10. Measured (a) conversion gain versus IF frequency when LO frequency was fixed at 15 GHz and (b) conversion gain versus RF frequency for different IF frequencies in downconversion.

were 16 GHz and 17 dBm, respectively. The optical spectra of the lower branch and upper branch were shown in Fig. 8(a) and (b). As can be seen, a sideband suppression ratio of 24.8 dB and a carrier suppression ratio of 22.3 dB can be acquired. As in the upconversion mode, the +1st-order sideband of the RF signal and the LO signal were selected by the tunable OBPF.

The electrical spectra of the downconverted IF were measured when the LO frequency was fixed at 15 GHz and the RF frequency was adjusted from 16 to 40 GHz. As can be seen in Fig. 9(a), the spurs suppression ratio still exceeded 50 dB within the measured frequency range of 0-40 GHz. Fig. 9(b) shows the SFDR for downconversion, the two-tone RF frequencies were 17 GHz and 17.1 GHz and the LO frequency was 10 GHz. As can be seen, a noise floor at -160 dBm/Hz was assumed, and the SFDR was about 110.39 dBc·Hz$^{2/3}$.

The conversion gain as a function of IF frequency was measured in Fig. 10(a) when the parameter settings were consistent with Fig. 9(a). The conversion gain remained around −33 dB with a fluctuation of 2 dB. Furthermore, conversion gain as a function of RF frequency for different IF frequencies was shown in Fig. 10(b). As can be seen, the system facilitated a broad operating frequency range of 8 to 40 GHz for downconversion, all while maintaining a consistent conversion gain with fluctuation of less than 1.3 dB. Nevertheless, the operating bandwidth was limited by the bandwidth of the PD used in the experiment.

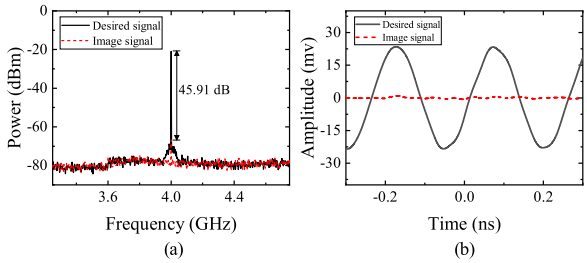

Fig. 11. Measured (a) spectra and (b) waveforms of the downconverted IF from desired RF (black solid line) and undesired image (red dashed line).

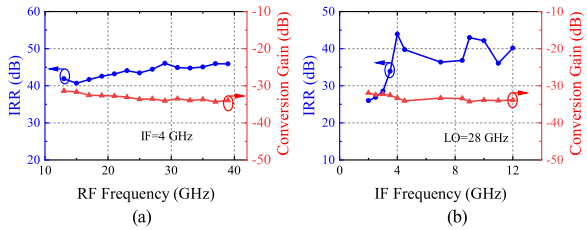

Fig. 12. Measured IRR (blue dots) and conversion gain (red triangles) versus (a) RF frequency and (b) IF frequency.

C. Pre-Filtering Based Image Rejection Mixer

To showcase the image rejection performance of the proposed scheme, the LO frequency was set to 35 GHz, and the RF frequency was set to 39 GHz, the corresponding downconverted IF was at a frequency of 4 GHz. Subsequently, the RF signal was switched to the image signal at 31 GHz and applied to the upper I/Q modulator. The measured electrical waveforms and spectra of the downconverted IF from the desired RF and undesired image were depicted in Fig. 11(a) and (b). It can be seen that the IRR of the proposed IRM was about 45.91 dB at an IF frequency of 4 GHz and the amplitude of the downconverted image product was nearly zero. It is noteworthy that a minor distortion is observed in the desired signal waveform in Fig. 11(b). This is attributed to the frequency of the modulated RF signal, which exceeds the operating bandwidth of the modulator (35 GHz), leading to a decrease in signal-to-noise ratio and subsequent waveform distortion.

The corresponding IRR and conversion gain were measured in Fig. 12(a) when the downconverted IF was fixed at 4 GHz and the RF frequency was adjusted from 13 to 39 GHz. An IRR of 46 dB can be achieved at an RF frequency of 29 GHz and the IRR within the measured frequency range was more than 40 dB, and the conversion gain remained around -33 dB with a fluctuation of 3 dB. The variation of IRR can be attributed to the uneven out-of-band suppression introduced by the employed OBPF. Furthermore, the corresponding IRR and the conversion gain were measured in Fig. 12(b) when the LO frequency was

fixed at 28 GHz and the downconverted IF frequency varied from 2 to 12 GHz. The IRR was more than 35 dB when the frequency of IF was greater than 4 GHz, in contrast to the 26 dB obtained at an IF frequency of 2 GHz, since the image signal cannot be completely suppressed when the frequency of the IF signal lower than the bandwidth of the OBPF. Additionally, the conversion gain hovered around -33 dB with a fluctuation of 2.4 dB.

D. Stimulated Brillouin Scattering-Based Image Rejection Mixer

To solve the problem that the IRR was reduced when the IF frequency decreased, which remained in the previously proposed scheme, an improved IRM based on a Brillouin-assisted notch filter was proposed. A new branch modulated by the RF pump wave was employed to generate the optical pump light. The loss spectrum of the pump light was used to attenuate the image signal. In this way, the reduction in IRR caused by the insufficiently suppressed image can be compensated.

Based on the original setup, an extra 50:50 OC was added to split a portion of the optical power for the generation of the pump light. The optical carrier was injected into the intensity modulator (THORLABS LN05S), which was driven by the RF pump wave. A bias control module (Plug Tech MBC-MZM) was employed to control the intensity modulator to bias at MITP to achieve CS-DSB modulation. The pump signal was amplified using an EDFA, which was followed by the polarization controllers (PC) to adjust the polarization state of the amplified pump light and signal light to maximize the SBS effect in the 10 km SMF (SMF-28). Following the adjustment of the PC1, the pump light was coupled to the SMF via a circulator (AFR PMCIR). In the middle branch which was modulated by RF and image signals, the CS-SSB signals were acquired using the previously mentioned method. After traversing through an isolator (AFR PMI), the forward-transmitted optical signal was directed into SMF via PC2. The SMF used in the experiment had a length of 10 km and a Brillouin frequency shift of 10.832 GHz. Upon interaction with the counter-propagating pump light in the SMF, the forward-transmitted optical signal was subsequently directed into the OBPF through the circulator. The branch responsible for generating the CS-SSB signal of the LO remained unaltered. An EDFA was applied to amplify the combined signal, and the optical signals were detected by a PD.

For the purpose of showcasing the enhancement in IRR relative to the previous scheme, the RF pump wave was set to 5.168 GHz and the image signal was set to 16 GHz located at the center of the loss spectrum. The center frequency of the OBPF was shifted by ∼4 GHz in relation to the image sideband, ensuring suppression of the image sideband. The optical spectra of the image sideband under different conditions were measured in Fig. 13(a). As can be seen, the original CS-SSB signal of the image was marked as black solid line, the red dashed line represented the signal solely suppressed by the OBPF, whereas the blue dotted line illustrated the signal suppressed by both the OBPF and the loss spectrum. Notably, the signal marked by the blue dotted line was attenuated to a level approaching

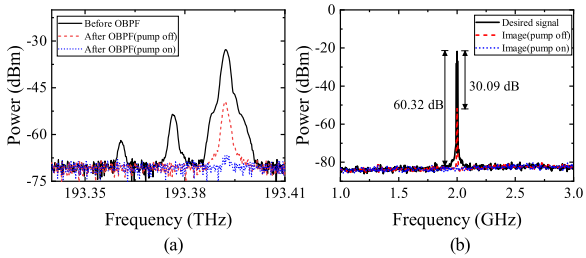

Fig. 13. Measured (a) optical spectra of the image sideband before OBPF (black solid line), after OBPF with pump off (red dashed line) and after OBPF with pump on (blue dotted line) and (b) electrical spectra of the downconverted IF from the desired signal (black solid line), from the image with pump off (red dashed line) and from the image with pump on (blue dotted line).

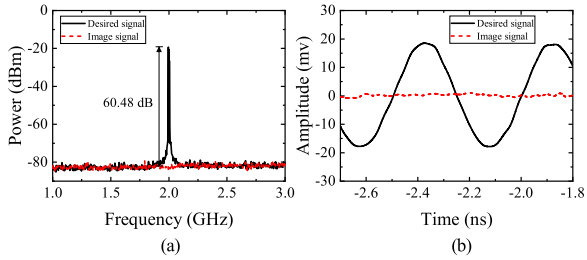

Fig. 14. Measured (a) spectra and (b) waveforms of the downconverted IF from desired RF (black solid line) and undesired image (red dashed line).

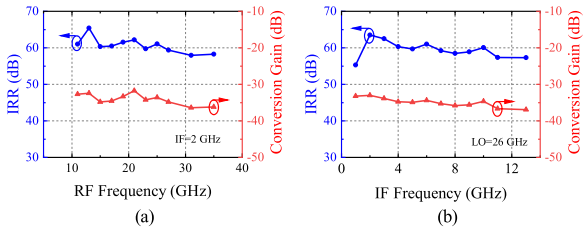

Fig. 15. Measured IRR (blue dots) and conversion gain (red triangles) versus (a) RF frequency and (b) IF frequency.

the noise floor. The electrical spectra of the obtained image product and useful IF signal under different conditions were measured in Fig. 13(b) when the RF frequency and LO frequency were set to 15 GHz and 13 GHz respectively, the corresponding downconverted IF at a frequency of 2 GHz. Subsequently, the RF signal was switched to the image signal at a frequency of 11 GHz. It can be seen that the IRR was 30.09 dB in the absence of the pump, whereas with the pump active, the IRR reached 60.32 dB, thus an improvement of 30.23 dB in IRR can be acquired.

The measured electrical waveforms and spectra of the obtained image product and useful IF signal were measured in Fig. 14(a) and (b) when the RF frequency and the LO frequency were 17 GHz and 15 GHz respectively, the corresponding downconverted IF was at a frequency of 2 GHz. Subsequently, the RF signal was switched to the image signal at a frequency of 13 GHz. As can be observed, the IRR of the proposed SBS-based IRM was about 60.48 dB at an IF frequency of 2 GHz and the amplitude of the downconverted image was nearly zero. Additionally, no distortion is observed in the waveform of the downconverted desired signal, as illustrated in Fig. 14(b).

The IRR and the conversion gain were measured in Fig. 15(a) when the RF frequency was adjusted from 11 to 35 GHz and the LO was adjusted from 9 to 33 GHz to obtain the IF signal at a frequency of 2 GHz. As can be seen, an IRR of 65 dB can be achieved at an RF frequency of 13 GHz. Additionally, the IRR was more than 58 dB across a wide RF frequency range and the conversion gain remained near -34 dB with a fluctuation of 4.6 dB. Furthermore, the LO frequency was fixed at 26 GHz, and the downconverted IF frequency varied from 1 to 14 GHz. The IRR and the conversion gain were measured in Fig. 15(b). The IRR was greater than 57.3 dB when the IF frequency was greater than 2 GHz. However, the IRR experienced a significant decline at an IF frequency of 1 GHz. This decrease occurred because the frequency of the image sideband fell in the passband of the OBPF, and the image signal almost only suffered attenuation from the loss spectrum of the pump. Nevertheless, an IRR of 55.3 dB was still achievable. In addition, the conversion gain hovered around -35 dB with a fluctuation of 3.6 dB. As shown in Fig. 14(a) and (b), the conversion gain was 1-2 dB lower than that in the unimproved scheme, which was caused by optical loss introduced by the 10 km SMF. Moreover, the fluctuation of conversion gain was higher than the unimproved scheme, since the system was susceptible to environmental variation due to the use of SMF. Despite this, since all the devices and patch cords used in this article are polarization-maintaining, the proposed system is capable of remaining immunity to the variation in polarization state and maintaining excellent stability.

IV. Conclusion

In this article, we have presented a microwave photonic mixer utilizing dual parallel I/Q modulators, enabling both up and down conversion with high performance. The upconversion process upconverts an IF frequency range of 5-17 GHz to an RF frequency range of 15-37 GHz, the downconversion permits an RF frequency range of 8-40 GHz to be downconverted to an IF frequency range of 2-5 GHz. The spurs suppression ratio reaches ∼50 dB for both up and down conversion. To the best of our knowledge, this is the highest reported spur suppression in a broadband microwave photonic mixer. Additionally, an IRR of 45.91 dB at an IF frequency of 4 GHz is obtained via the OBPF. For achieving a lower frequency of downconverted signal and a higher IRR, a Brillouin-assisted notch filter is applied to achieve an IRR of more than 60 dB at an IF frequency of 2 GHz. Thanks to the high spurs suppression and IRR, the proposed mixer can find applications in radar receiver, RoF system, electronic warfare, and satellite payload.

References

[1] P. Ghelfi et al., "A fully photonics-based coherent radar system," *Nature*, vol. 507, pp. 341–345, Mar. 2014.

[2] S. Pan et al., "Satellite payloads pay off," *IEEE Microw. Mag.*, vol. 16, no. 8, pp. 61–73, Sep. 2015.

[3] F. Laghezza, F. Scotti, P. Ghelfi, and A. Bogoni, "Photonics-assisted multi-band RF transceiver for wireless communications," *J. Lightw. Technol.*, vol. 32, no. 16, pp. 2896–2904, Aug. 2014.

[4] Y. Gao, A. Wen, W. Jiang, Y. Fan, and Y. He, "All-optical and broadband microwave fundamental/sub-harmonic I/Q down-converters," *Opt. Exp.*, vol. 26, no. 6, pp. 7336–7350, 2018.

[5] S. T. Lipkowitz, T. U. Horton, and T. E. Murphy, "Wideband microwave electro-optic image rejection mixer," *Opt. Lett.*, vol. 44, no. 19, pp. 4710–4713, Oct. 2019.

[6] G. K. Gopalakrishnan, W. K. Burns, and C. H. Bulmer, "Microwave-optical mixing in LiNbO3 modulators," *IEEE Trans. Microw. Theory-Techn.*, vol. 41, no. 12, pp. 2383–2391, Dec. 1993.

[7] Z. Tang, F. Zhang, D. Zhu, X. Zou, and S. Pan, "A photonic frequency downconverter based on a single dual-drive Mach-Zehnder modulator," in *Proc. IEEE Int. Topical Meeting Microw. Photon.*, 2013, pp. 150–153.

[8] E. H. W. Chan and R. A. Minasian, "Microwave photonic downconverter with high conversion efficiency," *J. Lightw. Technol.*, vol. 30, no. 23, pp. 3580–3585, Dec. 2012.

[9] Z. Tang and S. Pan, "Reconfigurable microwave photonic mixer with minimized path separation and large suppression of mixing spurs," *Opt. Lett.*, vol. 42, no. 1, pp. 33–36, Dec. 2017.

[10] Z. Tang and S. Pan, "A reconfigurable photonic microwave mixer using a 90° optical hybrid," *IEEE Trans. Microw. Theory Techn.*, vol. 64, no. 9, pp. 3017–3025, Sep. 2016.

[11] Y. Zhang et al., "Broadband image-reject mixing based on a polarization-modulated dual-channel photonic microwave phase shifter," *IEEE Photon. J.*, vol. 12, no. 2, Apr. 2020, Art. no. 7800409.

[12] Z. Shi, S. Zhu, M. Li, N. H. Zhu, and W. Li, "Reconfigurable microwave photonic mixer based on dual-polarization dual parallel-Mach–Zehnder modulator," *Opt. Commun.*, vol. 428, pp. 131–135, 2018.

[13] J. Li et al., "A microwave photonic mixer using a frequency-doubled local oscillator," *IEEE Photon. J.*, vol. 10, no. 3, Jun. 2018, Art. no. 5501210.

[14] Y. Gao et al., "An efficient photonic mixer with frequency doubling based on a dual-parallel MZM," *Opt. Commun.*, vol. 321, pp. 11–15, 2014.

[15] B. C. Henderson and J. A. Cook, "Image-reject and single-sideband mixers," Watkins-Johnson Company, Palo Alto, CA, USA, Tech. Rep. 18, 1985.

[16] A. C. Lindsay, G. A. Knight, and S. T. Winnall, "Photonic mixers for wide bandwidth RF receiver applications," *IEEE Trans. Microw. Theory Techn.*, vol. 43, no. 9, pp. 2311–2317, Sep. 1995.

[17] S. J. Strutz and K. J. Williams, "An 8–18-GHz all-optical microwave downconverter with channelization," *IEEE Trans. Microw. Theory Techn.*, vol. 49, no. 10, pp. 1992–1995, Oct. 2001.

[18] S. J. Strutz and K. J. Williams, "A 0.8–8.8-GHz image rejection microwave photonic downconverter," *IEEE Photon. Technol. Lett.*, vol. 12, no. 10, pp. 1376–1378, Oct. 2000.

[19] X. H. Cao et al., "Filter-free photonic microwave I/Q modulator for reconfigurable frequency mixing," *J. Lightw. Technol.*, vol. 41, no. 9, pp. 2707–2714, May 2023.

[20] Y. Gao et al., "Reconfigurable microwave photonic mixer for hybrid macro-micro cellular systems," *Opt. Exp.*, vol. 31, no. 4, pp. 5314–5333, 2023.

[21] J. Zhang, E. H. W. Chan, X. Wang, X. Feng, and B. Guan, "High conversion efficiency photonic microwave frequency converter with image rejection capability," *IEEE Photon. J.*, vol. 8, no. 4, Aug. 2016, Art. no. 3900411.

[22] D. Shan et al., "Filter-free image-reject microwave photonic downconverter based on cascaded modulators," *Appl. Opt.*, vol. 58, no. 13, pp. 3432–3437, May 2019.

[23] Z. Tang and S. Pan, "A compact image-reject and single-sideband mixer with suppression of LO leakage based on a dual-polarization dual-drive Mach-Zehnder modulator," in *Proc. IEEE Int. Topical Meeting Microw. Photon.*, 2016, pp. 79–82.

[24] W. Zhang, A. Wen, Y. Gao, S. Shang, H. Zheng, and H. He, "Large bandwidth photonic microwave image rejection mixer with high conversion efficiency," *IEEE Photon. J.*, vol. 9, no. 3, Jun. 2017, Art. no. 7201908.

[25] Z. Zhu, D.-Y. Choi, S. Madden, B. J. Eggleton, and M. Merklein, "High-conversion-gain and deep-image-rejection Brillouin chip-based photonic RF mixer," *Opt. Lett.*, vol. 45, no. 19, pp. 5571–5571, Sep. 2020.

[26] K. Zhai, S. Zhu, and N. Zhu, "Stimulated Brillouin scattering based image reject microwave signal harmonic down-converter," *IEEE Photon. J.*, vol. 14, no. 6, Dec. 2022, Art. no. 5556306.

[27] L. McKay et al., "Chip-based SBS for image rejection in a broadband microwave photonic mixer," *Opt. Exp.*, vol. 31, no. 3, pp. 4268–4280, Jan. 2023.

[28] X. Kong, Y. Yu, H. Tang, and X. Zhang, "Microwave photonic image-reject mixer based on a tunable microwave photonic filter with high rejection," *IEEE Photon. J.*, vol. 10, no. 6, Dec. 2018, Art. no. 5502411.

[29] C. B. Albert, C. Huang, and E. H. W. Chan, "Brillouin-assisted notch filtering based all-optical image rejection mixer," *IEEE Photon. J.*, vol. 11, no. 2, Apr. 2019, Art. no. 7202712.

[30] D. Marpaung, J. Yao, and J. Capmany, "Integrated microwave photonics," *Nature Photon.*, vol. 13, no. 2, pp. 80–90, Feb. 2019.